Roles of core-shell and δ-ray kinetics in layered BN α-voltaic efficiency

Corey Melnick,[1] Massoud Kaviany,[1,2] and Moo-Hwan Kim[2]
[1]*Mechanical Engineering Department, University of Michigan, Ann Arbor, Michigan 48109, USA*
[2]*Division of Advanced Nuclear Engineering, POSTECH, Pohang 790-784, South Korea*

(Received 10 December 2012; accepted 22 January 2013; published online 11 February 2013)

α-voltaics harvest electron-hole pairs created as energetic α particles collide with and ionize electrons in a semiconductor, creating δ-rays. After ionization, charged pair production continues through δ-ray impact ionization events and the Auger relaxation of core-shell holes created through K-shell ionization events. Secondary ionization events are quantified using the TPP-2M model, the fraction of K-shell ionization events is determined using the energy-loss Coulomb-repulsion perturbed-stationary-state relativistic theory, and the relaxation of the resulting holes is treated with a fully *ab initio* approach using multiple Fermi golden rule calculations for ranges of carrier concentrations and temperatures. The limiting rate is $15\,ns^{-1}$ for small carrier concentrations and high temperatures, as compared to the radiative core-shell relaxation rate estimated here at $20\,ns^{-1}$, indicating that Auger modes contribute significantly. Moreover, the K-shell ionization events are shown to dominate for low energy α particles and vanish for high energy ones. Thus, the efficiency loss due to energy dissipation in the fuel layer is mitigated, which is demonstrated by the analysis of a layered fuel-voltaic device with an efficiency from 20% to 14% for fuel layers between 5 and 10 μm thick. The design of a α-voltaic integrated with a thermoelectric generator is suggested for improved efficiency and the system-level mitigation of radiation damage and geometric inefficiency. © *2013 American Institute of Physics*. [http://dx.doi.org/10.1063/1.4790506]

I. INTRODUCTION

In α-voltaics, α particles from a source, e.g., Pu-238, collide with and ionize electrons in a semiconductor. Ionized electrons, i.e., δ-rays, move through the material colliding elastically and inelastically with atoms, inducing further ionization events, and interacting with the lattice, emitting (and absorbing) phonons. The two relaxation modes are comparable only around the ionization threshold energy (typically around 1.5 times the bandgap), above which ionization events are orders of magnitude faster and more energetically, and below which the ionization rates drop precipitously. Ionization events occur in both inner (K) and valence shells (L). Holes left in the L shell relax to the valence band-edge via multiple phonon emissions, while holes in the K shell must relax to the L shell through either Auger [electron-electron-hole (*e-e-h*)] or radiative [photon (*ph*)] interactions. These relaxation paths are shown in Fig. 1. The fraction of K-shell ionization events that relax via Auger modes and secondary δ-ray ionization events increase the system efficiency, while phonon emissions generate "waste" heat. However, because the α-voltaic is a direct energy conversion (DEC) cycle (i.e., it is not a thermal cycle), a thermal cycle, e.g., a thermoelectric generator (TEG), can be added to the α-voltaic system, which is said to "top" the TEG.

Cress[5] provides a thorough analysis of radiation damage and efficiency in InGaP, including losses to non-active regions and optimizes *nipi* junctions for both damage mitigation and power generation. However, the number of electrons generated per α particle is determined experimentally. Other semi-empirical α-voltaic efficiency studies include the results of Klein,[6] who showed that the energy required to create a single electron-hole pair after all secondary ionization events

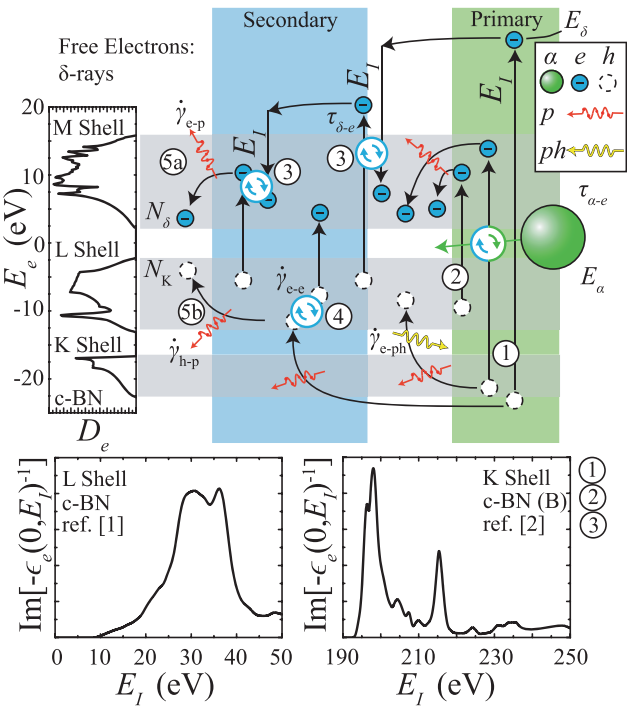

FIG. 1. The ionization and relaxation of electrons in an α-voltaic. Primary K (1) and L-shell (2) ionization events, secondary δ-ray impact ionization events (3) and Auger K-shell hole relaxation (4), as well as nonradiative relaxations ((5a) and (5b)): electron and hole phonon emissions) are shown. These interactions describe the manner in which charged-pairs are generated in an α-voltaic. The density of states (D_e) for c-BN and the ELFs $[-\epsilon(0,E_l)^{-1}]$ for c-BN at the L[1] and K-shell[2] (boron) edges. The latter are used in the TPP-2M model[3,4] to describe impact ionization (3) and can be extended to the primary ionizations (1,2). Here, the fraction of (1) to (2) is determined with ECPSSR theory.

occur is approximately $2.8\Delta E_g + 0.05$. This simple relation offers impressive accuracy for most semiconductor targets and particles studied, and a small sample of the use of this in α and β voltaic is provided in Refs. 7–10. Ziaja *et al.*[11–13] take a theoretical Monte Carlo (MC) approach to quantify the energy required by ionizing electrons to create an electron-hole pair in diamond. Scattering cross sections and mean-free paths from many studies are used to describe the many regimes and phenomena in δ-ray electron showers, including electron and hole impact ionization and core-shell involvement. Their predicted result (13.3 eV) lies among experimental values and slightly below the value predicted by the relation of Klein (15 eV). We attempt to reproduce similar success without relying on the often opaque nature of MC methods. We calculate the *ab initio* core-shell kinetics and singly differentiable scattering cross sections to facilitate this. Finally, we illustrate the interplay among device geometry, efficiency, and underlying physics.

Cubic boron nitride (c-BN) is chosen here for (i) its low atomic number allowing core-shell effects, (ii) promise for fundamental studies, and (iii) promise as an α-particle material. However, our methods should be applicable to any α-voltaic material, and in addition to theory, we will address the device and improved efficiency.

II. EFFICIENCY

The energy of a primary ionization event (E_I) preserved by an α-voltaic is $N\Delta E_{e,g}$, where N is the number of electron-hole pairs generated through subsequent δ-ray impact ionization (N_δ) or core-shell hole ($N_{h,\mathrm{K}}$) Auger relaxation events per primary ionization, and $\Delta E_{e,g}$ is the bandgap. Thus, the efficiency of a single ionization event η_I is

$$\eta_I = (N_\delta + N_{h,\mathrm{K}})\frac{\Delta E_{e,g}}{E_I}. \tag{1}$$

For a probability distribution of primary ionization events $P_{I,\alpha,i}(E_I)$ in the $i = \mathrm{K}$ or L bands, the ionization efficiency of shell i ($\eta_{I,i} = \eta_{\delta,i} + \eta_{h,i}$) is

$$\eta_{\delta,i} = \int_0^\infty \frac{\Delta E_{e,g}}{E_I} N_{\delta,i}(E_I) P_{I,\alpha,i}(E_I)\mathrm{d}E_I, \tag{2}$$

$$\eta_{h,i} = \int_0^\infty \frac{\Delta E_{e,g}}{E_I} N_{h,i}(E_I) P_{I,\alpha,i}(E_I)\mathrm{d}E_I, \tag{3}$$

and the maximum efficiency is

$$\eta_{\max} = P_L\eta_{I,\mathrm{L}} + P_K\eta_{I,\mathrm{K}}, \tag{4}$$

where P_i is the probability of an ionization event by an α particle with energy E_α.

Thus, we need to model $N_{\delta,i}$, $N_{h,\mathrm{K}}$, and $P_{I,\alpha,i}$ as a function of E_I in order quantify η_I and P_i in order to combine the results. The $\delta - e$ kinetics ($\tau_{\delta-e}$) govern $N_{\delta,i}$, the $e - e$ kinetics ($\dot{\gamma}_{e-e}$) govern $N_{h,\mathrm{K}}$, and the $\alpha - e$ kinetics ($\tau_{\alpha-e}$) govern $P_{I,\alpha,i}$. The Tanuma-Powell-Penn model (TPP-2M)[3,4] model is used to calculate $\tau_{\delta-e}$ and $\tau_{\alpha-e}$ in Sec. III, and we perform *ab initio* Fermi golden rule calculations to determine $\dot{\gamma}_{e-e}$ in Sec. V. The accurate energy-loss coulomb-repulsion perturbed-stationary-state relativistic (ECPSSR) theory[14] is used to determine P_i in Sec. IV. We begin with the a description of electron showers ($N_{\delta,i}$, $P_{I,\alpha,i}$, and $\eta_{\delta,i}$).

III. ELECTRON SHOWER

In order to determine $N_{\delta,i}$, we must account for the inelastic interactions between a primary δ-ray and the lattice (phonon emission and absorption) and bound electrons. In general, ionization events dominate for energetic δ-rays with energy greater than approximately $1.5\Delta E_{e,g}$ (the ionization threshold) while intervalley and optical phonon emission dominates below this threshold (Fig. 1). The region between these domains, where δ-rays couple to phonons and electrons is narrow and begins at the ionization threshold energy E_t, after which the electron-electron interaction rate increases by many orders of magnitude within a few eV. Unified and rigorous models for $N_{\delta,i}$ and E_I which include this region (e.g., <10 eV) and extend into the high energy domain are unavailable. Here, we use the TPP-2 M model to describe the kinetics for $E_\delta > E_t$ and assume δ-rays below the threshold lose all remaining kinetic energy to the lattice. Before continuing, we outline the basis of the TPP-2M model.

Fermi[15] modeled the linear perturbations caused by the electric field of a fast charged particle. Subsequent studies built on this to incorporate many of the quantum-mechanical effects,[16–18] and such models have been successfully used in a similar analysis of electron showers in diamond.[11–13] The linear response of a solid to an electric field is characterized by the dielectric function $\epsilon_e(\boldsymbol{k}_I, E_I)$, where $\hbar\boldsymbol{k}_I$ and $\hbar E_I$ are the momentum and energy transfer in the interaction. Under this approximation, the energy loss of the charged particle $\mathrm{d}E/\mathrm{d}t$ is proportional to the double integral of $\mathrm{Im}[-\epsilon_e(\boldsymbol{k}_I, E_I)^{-1}]$.[19] Thus, the dielectric function enables calculation of $\tau_{I,i}(E_\delta, E_I)$. Moreover, at high energies, the ionization kinetics of different charged particles are equal,[20] and we can use the dielectric function to calculate $\tau_{\alpha,e}(E_\delta, E_I)$ and $P_{I,\alpha,i}$.

In general, it is much easier to calculate the energy loss function (ELF) $\mathrm{Im}[-\epsilon_e(0, E_I)^{-1}]$ (i.e., for photo-ionization) and then extend the ELF to an arbitrary wavenumber $\boldsymbol{k}_I$. The TPP-2M uses statistical considerations to successfully extend $\mathrm{Im}[-\epsilon_e(0, E_I)^{-1}]$ to arbitrary wavenumbers and energies in order to calculate the differential and total inelastic mean free paths (DIMFP and IMFP) of electrons in semiconductors. In this model, the inverse DIMFP $\tau_I(E_\delta, E_I)$ for an electron in atomic units where $\hbar = m_e = e_c$ is

$$\begin{aligned}\tau_I(E_\delta, E_I) &= \frac{1}{2\pi E_\delta}\int_{E_-}^{E_+} \mathrm{d}E_I' E_I' \mathrm{Im}[-\epsilon_e(0, E_I)^{-1}] \\ &\times \frac{1}{[c(E_I')^2 - E_I'^2 + E_I^2]^{1/2}\{[c(E_I')^2 - E_I'^2 + E_I^2]^{1/2} - c(E_I')\}},\end{aligned} \tag{5}$$

where $c(E_I') = k_\mathrm{F}(E_I')^2/3$, and $k_\mathrm{F}(E_I') = (3\pi/4)^{1/3}E_I'^{2/3}$ is the Fermi wave number for a free-electron gas with plasma

frequency $E_I'/\hbar$.[12] The integration limits are solutions to the implicit equation

$$k_{\pm}^2/2 = (c(E_{\pm}')^2 - E_{\pm}'^2 + E_I^2)^{1/2}, \quad (6)$$

where $k_{\pm} = k_\delta[1 \pm (1 - \hbar E_I/E_\delta)^{1/2}]$ are the wavenumber transfer limits and k_δ is the wavenumber for a δ-ray (free electron) of energy E_δ (Fig. 2).

Calculations incorporating the full detail of the electronic density of states (D_e) and $\tau_I(E, E_I)$ are best left to Monte Carlo methods, as in the works of Ziaja *et al.*[11–13] However, such an approach requires not only an *ab initio* description of core-shell hole kinetics, but also the L-shell holes and M-shell electrons (<10 eV), where higher energy models, e.g., the TPP-2M model, provide unreliable results. These calculations and the MC analysis are left for future study. Here, the mean behavior is utilized for the tertiary ionization kinetics and the location of the ionized electron in the K or L-shell band. While this method sacrifices accuracy, the results are reasonable and allow for insight, such that its use is merited. The assumptions and method of our calculations described next.

We assume the following: (i) The valence and core electrons which are ionized by primary δ rats are selected from the energy averaged state in shell i ($\bar{E}_i$). (ii) The inelastic interaction only produces an electron-hole pair if $\bar{E}_I(E_\delta) > \Delta_{e,g} + \bar{E}_i$. (iii) Energy losses to the lattice are negligible above the ionization threshold and dominant below it. This assumption is naturally enforced by assumption (i), as $\Delta E_{e,g} + \bar{E}_L$ is larger than the ionization threshold, such that the transition region from negligible to dominant δ ray-lattice scattering is not reached. (iv) The tertiary impact ionization events transfer the mean ionization energy $\bar{E}_{I,L}$, the energy transfer at which half of all ionizations are less energetic.

The method is as follows: (i) Evaluate the mean electron energy from the valence bandedge for the K and L-shell bands $\bar{E}_i$. (ii) Calculate $\tau_{I,\delta,i}(E_\delta, E_I)$. (iii) Evaluate the mean ionization energy for variations in the δ-ray energy [$\bar{E}_{I,L}(E_\delta)$]. (iv) Determine the energies for which a primary δ-ray, through average interactions, creates one ($E_{i,1}$), two ($E_{i,2}$), or etc., additional electrons, where after each impact, the δ-ray transfers $\bar{E}_{I,L}(E_\delta)$ and the impacted electron is left with $\bar{E}_{I,L}(E_\delta) - \Delta E_{e,g} + \bar{E}_i$ kinetic energy. (v) Construct a function representing the number of electron-hole pairs generated through impact ionization of energy E_I by a primary δ ray

$$N_{\delta,i}(E_I) = 1 + \mathrm{H}(E_I - E_{i,1}) + \mathrm{H}(E_\delta - E_{i,1}) + \cdots, \quad (7)$$

where H is the Heaviside step function. (vi) Let $\tau_{I,\alpha,i} = \tau_{I,\delta,i}$ for $E_\delta \gg 300$ KeV, such that the probability distribution of primary ionizations $P_{I,\alpha,i}$ is

$$P_{I,\alpha,i} = \frac{\tau_{I,\delta,i}E_I}{\int_0^\infty \tau_{I,\delta,i}E_I \mathrm{d}E_I}. \quad (8)$$

The efficiency $\eta_{\delta,i}$ follows from Eqs. (2), (7), and (8)

$$\eta_{\delta,i} = \int_0^\infty \frac{\Delta E_{e,g}}{E_I}[1 + \mathrm{H}(E_I - E_{i,1}) + \mathrm{H}(E_\delta - E_{i,1}) + \cdots] \times \frac{\tau_{I,\delta,i}E_I}{\int_0^\infty \tau_{I,\delta,i}E_I \mathrm{d}E_I}\mathrm{d}E_I. \quad (9)$$

The results are presented below, following the steps listed above. Using DFT code VASP[21–24] with PAW-PBE (projector augmented wave generated by Perdew Burke, and Ernzerhof) pseudopotentials,[25–28] we generate D_e and calculate $\bar{E}_L = 4.8$ and $\bar{E}_K = 16.17$ eV. $\tau_{I,\delta,L}$ and $\bar{E}_{I,L}$ are evaluated for $10 < E_\delta < 500$ eV, at which point the change in $\bar{E}_{I,L}$ becomes negligible, using a theoretical ELF.[1] Similarly, $\tau_{I,\delta,L}$ and $\bar{E}_{K,K}$ are evaluated from $195 < E_\delta < 1000$ eV, using a theoretical ELF at the boron K-shell edge.[2] (We use the boron edge, because it is the dominant target for K-shell ionization events). $\bar{E}_{I,L}$ and $\bar{E}_{I,K}$ are presented in Fig. 2 with additional constant probability lines. This figure shows that $\bar{E}_{I,L}$ approaches 32 eV, slightly above ionization energies of L-shell electrons in boron and nitrogen, while 95% of all ionization events are less than 70 eV at high energies. Similarly, K-shell ionization events approach a mean energy transfer of 210 eV, slightly above the ionization energy of K-shell electrons in Boron, while the likelihood of a high energy ionization event increases significantly in contrast to a L-shell ionization event. This is due to the narrow K-Shell edge ELF. Next, we find $E_{L,i}$ and $E_{K,i}$, these values are presented in the supplementary materials.[29] From Eq. (9), $\eta_{\delta,L}$ is 38.8% and $\eta_{\delta,K}$ is 39.1%. In comparison, the Klein relation leads to an efficiency of 34.7%.

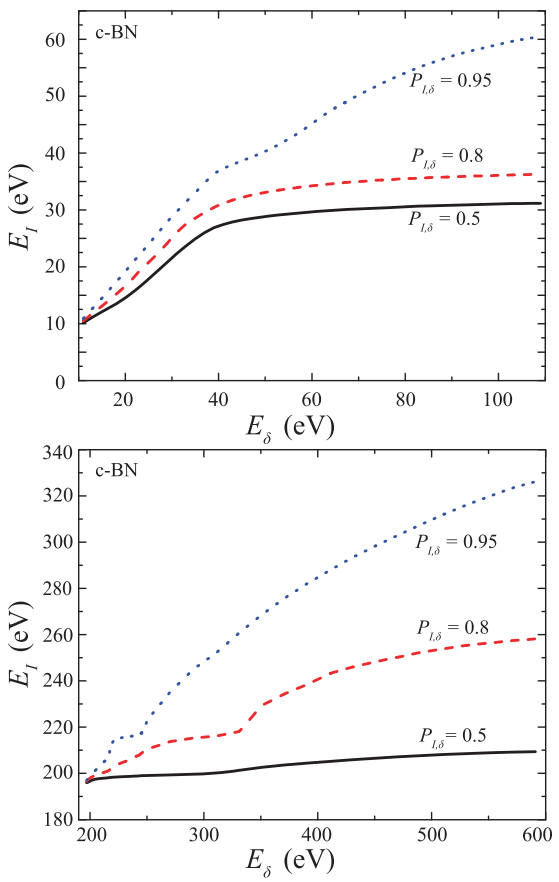

FIG. 2. Variations in $P_{I,\delta}(E_I, E_\delta)$, the probability that a δ ray of energy E_δ causes an ionization with energy less than or equal to E_I, for L (top) and K (bottom) shells. Probabilities of 0.5, 0.8, and 0.95 are shown.

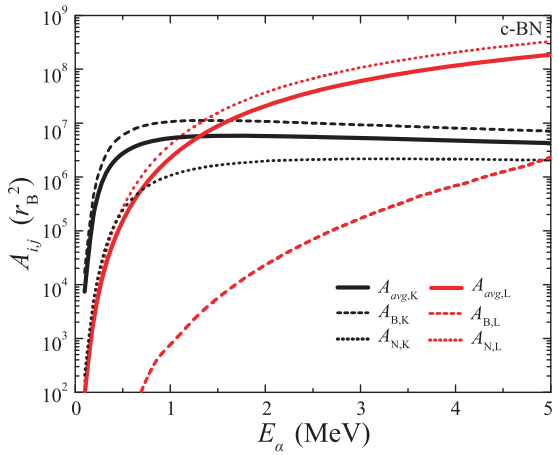

FIG. 3. Variations in the ionization cross sections (in atomic units) for boron, nitrogen, and boron nitride as a function of α particle energy (using ECPSSR theory as implemented by ISICS). As it shows, K-shell and boron interactions will dominate for small E_α, and L-shell and nitrogen interactions will dominate for large E_α.

We provide an illustration of this model failing. K-shell ionization events can generate highly energetic δ-rays that generate over 12 total electron-hole pairs through impact ionization events in this model; However, no quaternary ionization events can occur. In reality, quaternary electron-hole pairs, although rare, are generated by energetic primary δ-rays. The MC method can trace an electron through the required conditions, e.g., secondary δ-rays impacting electrons close to the valence band-edge and transferring a large energy E_I. However, the MC method can also trace electrons such that far fewer electron-hole pairs are created, e.g., if the primary δ ray impacts electrons deep in the valence band with insufficient energy to generate a secondary electron-hole pair. We use $\bar{E}_{I,i}$ and $\bar{E}_i$ with the aim of balancing between these extremes. By comparison with the Klein prediction, we can expect that this model underestimates the number of ionization events which fail to create electron-hole pairs; however, it is not conclusive. Experimental and MC analysis are required to support this supposition and are left for future studies.

Next, we calculate P_L and P_K.

IV. K AND L-SHELL IONIZATION

The relative probability of an L or K-shell ionization (P_L and P_K) is quantified by a mass-weighted sum of the component-atom ionization cross sections. Typically, L-shell interactions are dominant: As seen in, e.g., the similarities in behavior between InGaP α-voltaic and photovoltaic[5] and understood by both the outer electrons screening the K shell and also by the large ratio of outer to inner-shell electrons. However, in boron, there is weaker screening and only one more L than K-shell electron. Moreover, the coupling between inner electrons and α-particles without screening dominates at lower α-particle energies, such that K-shell ionization events can dominate the L-shell ionization events in boron, as shown in Fig. 3. Small increases in the atomic number (and the number of outer shell electrons), e.g., from B to N, significantly diminish inner shell involvement. Thus, the contribution of B (and the K shell) dominates at lower α-particle energies, while the contribution of N (and the L shell) dominates at higher energies. These cross sections are evaluated using ECPSSR with the united atom,[30] Hartree-Slater,[30,31] and relativistic core[32] corrections using the ISICS (Inner-Shell Ionization Cross Sections) implementation.[31,33] The resulting P_K and $\langle P_K \rangle$ are shown in Fig. 4, where $\langle P_K \rangle$ is P_K averaged from energy E_α to zero. $\langle P_K \rangle$ accounts for the range of energy experienced by an α particle that initially has energy E_α. In the subsequent analysis, $\langle P_K \rangle$ is used in the efficiency analysis and referred to as P_K for brevity.

Next, we need to determine the fraction of core-shell ionization events that create an additional electron-hole pair through Auger interactions $N_{h,K}$ and incorporate this into the efficiency.

V. *AB INITIO* CORE-SHELL KINETICS AND EFFICIENCY

The ratio of Auger ($\dot{\gamma}_{e-e-h}$) to total [Auger and radiative ($\dot{\gamma}_{e-ph}$)] scattering rates for core-shell holes define $N_{h,K}$ by

$$N_{h,K} = \frac{\dot{\gamma}_{e-e-h}}{\dot{\gamma}_{e-e-h} + \dot{\gamma}_{e-ph}}. \tag{10}$$

To find $\dot{\gamma}_{e-e-h}$, we perform a Fermi Golden rule calculation.

The screened electron-electron Hamiltonian[34] is

$$H_{e-e} = \frac{1}{2}\sum_{ij\mu\nu} \left\langle ij \left| \frac{e_c^2}{\epsilon_o r} e^{r/\lambda} \right| \mu\nu \right\rangle a_i^\dagger a_j^\dagger a_\mu a_\nu, \tag{11}$$

where e_c is the electron charge, λ is the screening length, r is the distance between electrons, and ϵ_o is the free-space permittivity. Here, $\lambda = [4\pi n_e e_c^2/(\epsilon_o k_B T)]^{-1/2}$, where n_e is the carrier concentration and T is the temperature. $|ij\rangle$ and $|\mu\nu\rangle$ are $|n_1\boldsymbol{k}_1, n_2\boldsymbol{k}_2\rangle$ and $|n_1'\boldsymbol{k}_2', n_2'\boldsymbol{k}_2'\rangle$, respectively, where n is the band index, and $\boldsymbol{k}$ is the wave vector. Examples of these

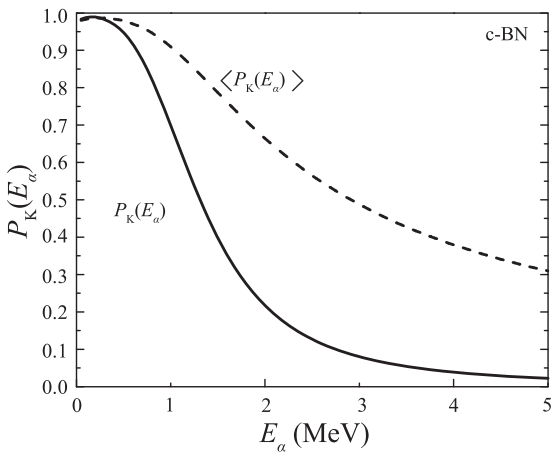

FIG. 4. Variations in P_K and $\langle P_K \rangle$ as a function of the E_α. As α particle slows down, it interacts more strongly with the core shell of boron and a large proportion of all ionization events create core-shell holes. The integrated probability $\langle P_K \rangle$ shows the average probability for an α-particle entering c-BN with energy E_α and illustrates the benefit of the strengthening core-shell interaction with decreasing particle energy.

states, the bandstructure and the auger relaxation mode are shown in Fig. 5.

The interaction matrix element is[34]

$$M_{ij\mu\nu} = \langle n_1'\boldsymbol{k}_1', n_2'\boldsymbol{k}_2'|\mathrm{H}_{e-e}|n_1\boldsymbol{k}_1, n_2\boldsymbol{k}_2\rangle = -\frac{4\pi e_c^2}{\epsilon_o\Omega}\frac{I^{n_2'\boldsymbol{k}_2'}_{n_1\boldsymbol{k}_1} I^{n_1'\boldsymbol{k}_1'}_{n_2\boldsymbol{k}_2}}{(\boldsymbol{k}_1-\boldsymbol{k}_2')^2+\lambda^{-2}}\delta(\boldsymbol{k}_1+\boldsymbol{k}_2-\boldsymbol{k}_1'-\boldsymbol{k}_2'), \tag{12}$$

where Ω is the Wigner-Seitz volume and the overlap integrals are

$$I^{n'\boldsymbol{k}'}_{n\boldsymbol{k}} = \int \psi_{n'\boldsymbol{k}'}(\boldsymbol{r})\psi_{n\boldsymbol{k}}(\boldsymbol{r})\mathrm{d}\boldsymbol{r}, \tag{13}$$

where $\psi_{n\boldsymbol{k}}(\boldsymbol{r})$ is the periodic part of the Bloch wavefunctions. From the Fermi golden rule, the relaxation rate of a hole from state μ in the K shell to i in the L shell is

$$\dot{\gamma}_{e-e-h,\mu} = \sum_{j\mu\nu}\frac{4\pi}{\hbar}|M_{ij\mu\nu}|^2 f_{e,i}f_{e,j}(1-f_{e,\mu}) \times \delta(E_{e,i}+E_{e,j}-E_{e,\mu}-E_{e,\nu}), \tag{14}$$

where f_e is the electron occupation, and j and ν are limited to the L and M shells, respectively. The scattering rate as a function of the K-shell hole energy, $\dot{\gamma}_{e-e-h}(E_{h,\mu})$, is summed over all μ with the same energy, while the overall scattering rate is summed over every state μ with the occupation $1-f_{e,\mu}$ included.

The initial states $(f_{e,i}, f_{e,j})$ are completely occupied, except near the Γ point. Similarly, the conduction band $(f_{e,\nu})$ is completely empty, except near the X valley. Assuming that intraband scattering dominates the interband scattering, core-shell holes will settle near the band edge at W and the occupation $f_{h,\mu}$ becomes

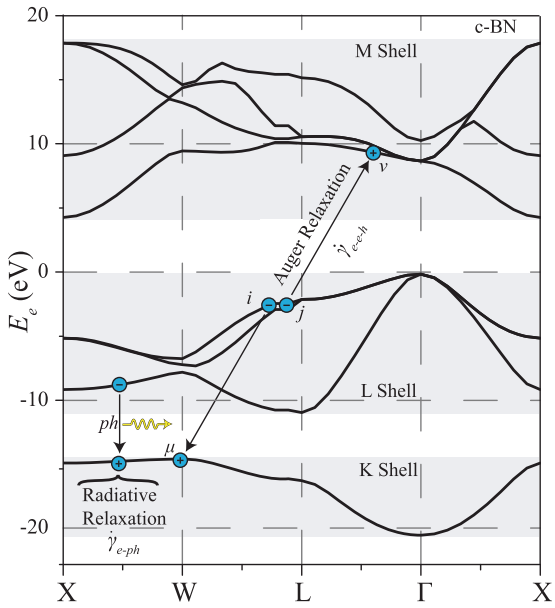

FIG. 5. The electronic bandstructure of cubic boron nitride (calculated using VASP). An example of Auger and radiative K-shell hole relaxation modes are shown with the initial (i, j) and final (μ, ν) Auger electron states indicated.

$$1-f_{e,\mu} = \frac{n_{h,\mathrm{K}}}{n_{\mathrm{K}}}\frac{1}{1+\exp(E_{h,\mu}/k_BT)}, \tag{15}$$

where $n_{h,\mathrm{K}}$ and n_{K} are the density of holes and the effective density of states in the K Shell, $E_{h,\mu}$ is the kinetic energy of a hole at state μ, and k_{B} is the Boltzmann constant. Combining Eqs. (12) to (15) with the occupancy assumptions, the resulting rate is

$$\dot{\gamma}_{e-e-h} = \frac{\pi}{\hbar}\left(\frac{8\pi e_c^2}{\epsilon_o\Omega}\right)^2\frac{n_{h,\mathrm{K}}}{n_{\mathrm{K}}}\sum_{ij\mu\nu}\frac{|I_i^\nu I_j^\mu|^2}{(|\boldsymbol{k}_i-\boldsymbol{k}_\nu|^2+\lambda^{-2})^2} \times \exp(-E_{h,\mu}/k_BT)\delta(\boldsymbol{k}_i+\boldsymbol{k}_j-\boldsymbol{k}_\mu-\boldsymbol{k}_\nu) \times \delta(E_i+E_j-E_\mu-E_\nu). \tag{16}$$

The details of this calculation are presented in the supplementary materials.[29]

The results of these calculations are presented in Fig. 6, and are discussed more thoroughly in the supplementary materials.[29] However, we emphasize from among these results the

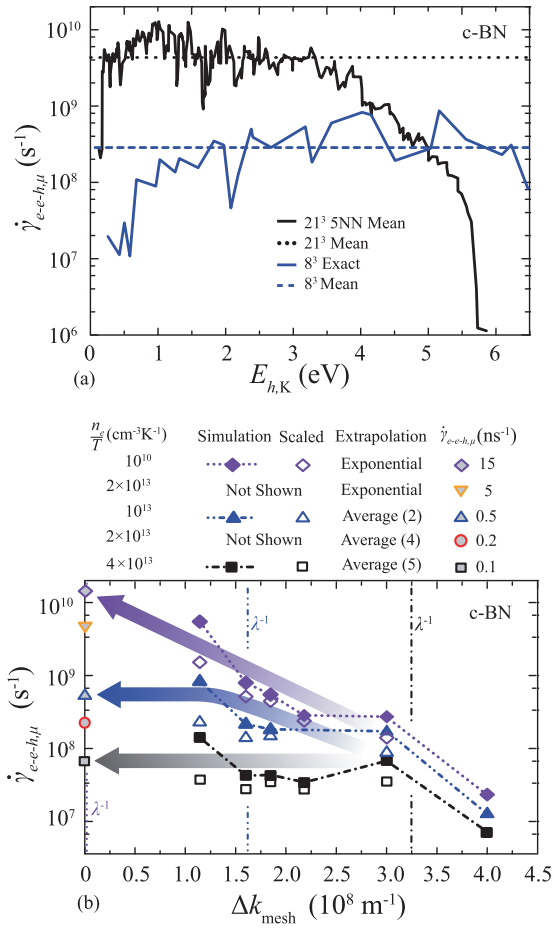

FIG. 6. (a) Variations of the Auger relaxation rate as a function of core-shell hole energy for 8^3 and 21^3 k meshes, where results for the latter are averaged among the five nearest neighbors. The average rates are also indicated. (b) Variations of the average Auger and scaled Auger relaxation rates as a function of Δk_{mesh} and n_e/T. Each λ^{-1}, extrapolated $\dot{\gamma}_{e-e-h,\mu}$, and extrapolation method for simulations with $n_e/T = 10^{10}, 10^{13}, 2\times10^{13}$, and 4×10^{13}cm^{-3}K^{-1} are listed. The parentheticals (2), (4), and (5) describe the number of convergent simulations with $\Delta k_{\mathrm{mesh}} < \lambda^{-1}$ averaged in order to quantify $\dot{\gamma}_{e-e-h,\mu}$. Note that the behavior at $\Delta k_{\mathrm{mesh}} \to 0$ represents the true behavior in the continuum.

limit $\dot{\gamma}_{e-e-h,\mu,avg} \leq 1.5 \times 10^{10} s^{-1}$ and note that $n_e/T \leq 5 \times 10^{10} cm^{-3} K^{-1}$ is sufficient to approach it. Next, we estimate the radiative relaxation rate in order to determine $N_{h,K}$ and η_{max}.

The interband radiative relaxation rate in semiconductors is approximately[35] $5 \times 10^7 \hbar\omega |M_p|$ (s^{-1}), where M_p is the momentum interaction matrix between initial and final states (eV), $\hbar\omega$ is the energy of the photon emitted (eV), i.e., the bandgap, and $M_p \approx 20$ eV.[35] There are three available bands above the K shell band-edge at W with energy gaps of 7.82, 7.36, and 6.76 eV. Therefore, the overall radiative relaxation rate is $\dot{\gamma}_{e-ph} \approx 20\, ns^{-1}$. Noting that both the Auger and radiative relaxation rates discussed neglect the hole occupancy, we can evaluate Eqs. (3) and (10) directly to find $N_{h,K}$, $\eta_{h,K}$ and $\eta_{I,K} = \eta_{h,K} + \eta_{\delta,K}$.

For high temperatures and low carrier concentrations ($n_e/T \leq 5 \times 10^{10} cm^{-3} K^{-1}$), N_K exceeds 0.4, which enhances the K-shell ionization efficiency by 1.1% (Eq. (3)), i.e., $\eta_{h,K} = 0.011$ and $\eta_{I,K} = 0.40$. The enhancement remains non-negligible up to $n_e/T = 2 \times 10^{12} cm^{-3} K^{-1}$, where $\dot{\gamma}_{e-ph} = 5 ns^{-1}$ and $N_{h,K} = 0.2$ ($\eta_{h,K} = 0.005$) before it quickly approaches zero with increasing n_e/T.

The device efficiency is reduced by the fraction of energy deposited in the fuel as opposed to the semiconductor, $1 - \eta_g$, where η_g is the geometric efficiency. To quantify η_g, we require $E_\alpha(x)$, the kinetic energy of a particle as a function of x and specify the device geometry. We calculate $E_\alpha(x)$, η_g, and the overall efficiency η_T next.

VI. LAYERED-DEVICE EFFICIENCY

The Bethe-Bloch stopping equation[36–38] models the kinetic energy of a particle E_α lost over a distance x, resulting in

$$\frac{\partial E_\alpha}{\partial x} = \frac{2\pi n_a z q_{\alpha,eff}^2 (m_\alpha/m_e)}{E_\alpha} \left(\frac{e_c^2}{4\pi\epsilon_o}\right)^2 \ln\left(\frac{4E_\alpha}{m_\alpha/m_e \Delta E_{e,\infty}}\right), \tag{17}$$

where n_a is the atomic number density the stopping material, $q_{\alpha,eff} = z_\alpha[1 - \exp(-u_\alpha/z_\alpha^{2/3} u_B)]^{1/2}$ is the effective charge of the particle,[39] m_α and m_e are the mass of the particle and electron, respectively. u_B is the Bohr velocity. Equation (17) is numerically integrated over x to find $E_\alpha(x)$. After a distance L_{es}, atomic stopping begins to dominate. The energy remaining at this point lowers the efficiency by $1 - \eta_{es}$, where $\eta_{es} = E_\alpha(0)/E_\alpha(L_{es}) = 0.95$. For an α particle stopping in c-BN, $L_{es} \approx 12.5\ \mu m$. (This is confirmed by more accurate Monte Carlo SRIM[40,41] calculations, which show good agreement throughout the remaining analysis).

The proposed device uses alternating layers of fuel and α-voltaic as shown in Fig. 7 to allow for both simple construction and reasonable efficiency. The semiconductor layer thickness $L_s = L_{es}$ so that all penetrating α particles complete their electronic stopping before exiting the α-voltaic layer. Neglecting layers separating the fuel and voltaic (which may be thin, not cover the entire layer, and have small stopping power), we derive the geometric efficiency, which includes the effect of $\eta_{max}(E_\alpha)$ and the increasing importance of K-shell ionization events with increasing L_f.

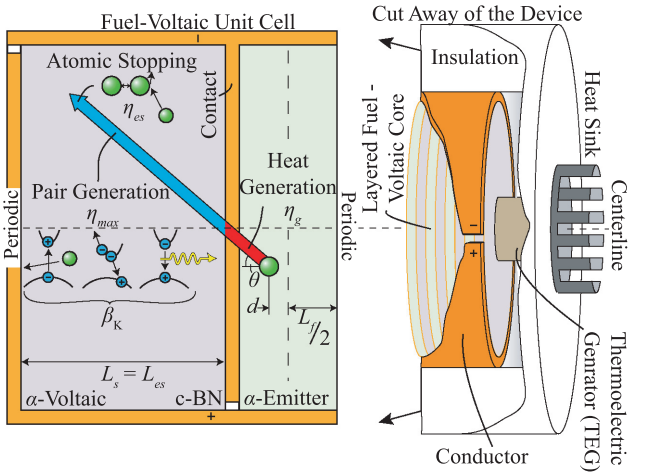

FIG. 7. A layered fuel-α-voltaic device integrated with a TEG. The device concentrates the heat generated in the device and funnels it through the TEG in order to meet its thermal requirements and maintain a reasonably efficient life-span.

The distance a particle has traveled is $x = (L_f/2 - d)/\cos(\theta)$ for $0 \leq \theta < \pi/2$ or $x = -(L_f/2 + d)/\cos(\theta)$ for $\pi/2 < \theta \leq \pi/2$, where d is the distance of emission from the fuel layer midline and θ is the polar angle of emission. $E_\alpha(x)$ follows from the integration of Eq. (17). The average $E_\alpha(x)$ reaching the semiconductor follows from an integration over the solid angles $\sin(\theta)\phi d\theta d\phi/(4\pi)$ and emission locations d/L_f. This is the end of a typical layered efficiency calculation. (For a similar discussion for a different geometry, see Ref. 5.) However, we saw in Sec. IV that the L and K-shell contributions are a function of the initial α-particle energy entering the semiconductor layer. Therefore, $\eta_{max} = P_L \eta_L + P_K \eta_K$ is interconnected with η_g and included in the integrand. Including symmetries, the geometric efficiency is

$$\begin{aligned}\eta_T = \eta_{es} \int_0^{\pi/2} \int_0^{L_f/2} \frac{1}{E_\alpha(0) L_f} \{ &\sin(\theta) E_\alpha[x(d,\theta)] (P_L \{E_\alpha[x(d,\theta)]\} \\ &\times \eta_{I,L} + P_K \{E_\alpha[x(d,\theta)]\} \eta_{I,K}) + \sin(\theta + \pi/2) \\ &\times E_\alpha[x(d,\theta+\pi/2)] (P_L \{E_\alpha[x(d,\theta+\pi/2)] \eta_{I,L} \\ &+ P_K \{E_\alpha[x(d,\theta+\pi/2)] \eta_{I,K}\}) \} d\theta dd. \end{aligned} \tag{18}$$

Figure 8 shows the geometric efficiency with (the overall efficiency) and without (an approximation of η_g) the L and K-shell contributions. While the higher K-shell efficiency (40% to the 38.8% of L-shell ionization events) and increasing K-shell contribution with fuel thickness acts to mitigate the losses in to the fuel, the difference is not sufficiently large for significant effect (an enhancement of only 0.5% is seen from $L_f = 1$ to 20 μm). We present a table of all relevant efficiency terms in Table I.

VII. RADIATION DAMAGE

The efficiency in Fig. 8 (e.g., 20% to 14% for fuel layers between 5 and 10 μm thick) includes primary and secondary ionization events and core-shell kinetics, and the energy deposited in the fuel as opposed to the voltaic. However, it

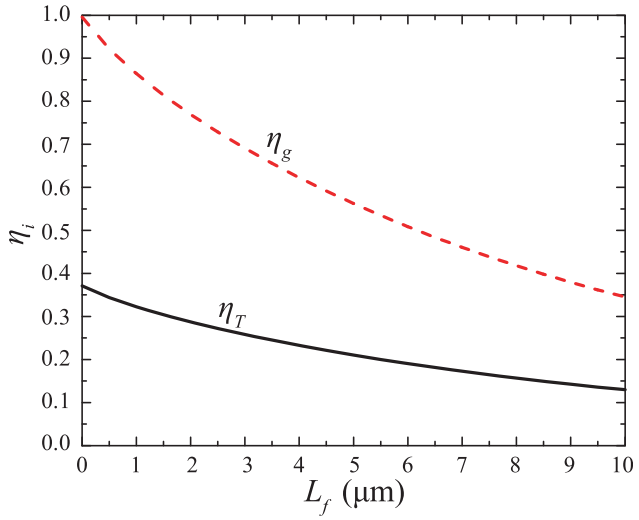

FIG. 8. Variations in the overall efficiency η_T and η_g for varying fuel layer thicknesses, L_f. Here, η_g is artificially separated from η_K and η_L, ignoring the non-linear interaction between the three terms, such that its rapid decay is illustrated.

does not account for radiation damage induced degradation, which is a serious concern. In a simple SiC device producing 15 nW/cm^2, the efficiency degrades to about 40% of its original value in 100 h when subjected to a plutonium source with an activity of 50 mCi.[7] While vacancies in c-BN are created with half the frequency (SRIM calculation) and the time constant for degradation may double that of SiC at high power densities, the radiation damage will quickly accumulate and long term operation restricts power fluxes. For example, a c-BN device operating above 60% of its initial efficiency for 1000 h would require a similar power flux. We note that the full effects of the displacements and vacancies on the efficiency degradation are not within the scope of this study, but we can expect that a similar or smaller efficiency loss will be seen due to its relative hardness, and electrical properties (e.g., the large bandgap should diminish the importance of trap assisted recombination), and a full study of the effects of radiation damage through replacements and vacancies, as well as the mitigation due to annealing, is left for future study.

VIII. BN α-VOLTAIC AS A TOPPING CYCLE

c-BN is a high temperature semiconductor, and *ab initio* molecular dynamics (AIMD) show that the bandstructure changes negligibly from 300 to 600 K (including the bandgap). Thus, we can achieve large $N_{h,K}$ with reasonable carrier concentrations using high temperatures. Moreover, we expect that negative effects including decreased mobility, increased recombination, and lowered bandgap will all have a smaller effect than $N_{h,K}$, because the mobility is sufficiently large, phonon-assisted radiative recombination is a generally weak function of temperature (and is likely to be the dominant recombination mode), and the bandgap changes negligibly according to our AIMD calculations. In fact, we assume that the temperature dependence of the efficiency, not including $N_{h,K}$, is negligible between, e.g., 300 and 600 K. Finally, there may be some annealing effects, which mitigate radiation damage at higher temperatures. For these reasons, high temperatures are desirable. This allows us to combine the DEC α-voltaic with TEGs, which tend to operate efficiently around 600 K (at, e.g., 8%). However, an efficient TEG design requires a heat flux on the order of mW/cm^2, around two orders of magnitude larger than that required for reasonably long term α-voltaic operation, as discussed in Sec. VII. Thus, a device concentrating the heat by two or more orders of magnitude is required. As an example, consider a core of layered fuel-voltaic elements sheathed in copper and encapsulated in insulation (see, Fig. 7). The copper conducts heat to a TEG with a heat sink on the cold side, such that its operational requirements are met, and it collects and conducts electricity out of the layered device. With such a device the efficiency will combine linearly, such that the maximum efficiency is 45%. Moreover, the TEG mitigates the effects of radiation damage and heat generation within the fuel. That is, if the efficiency has degraded by 50% in a device with 10 μm fuel layers, the TEG doubles system efficiency from 7% to 15%.

TABLE I. List of the relevant efficiencies, their values, and selected, influential terms. $\eta_{h,L}$ is zero by assumption. η_g and η_T are for $L_f = 5$ to 10 μm.

$\eta_{I,L}$	0.38	η_{es}	0.95
$\eta_{\delta,L}$	0.38	P_K	0.3 to 1
$\eta_{I,K}$	0.40	P_L	$1 - P_K$
$\eta_{\delta,K}$	0.39	η_g	0.5 to 0.35
$\eta_{h,K}$	0.01	η_T	0.20 to 0.14

IX. CONCLUSION

We develop methods for the theoretical evaluation of α-voltaic efficiency, including a semi-analytical description of the electron shower and an *ab initio* calculation of the core-shell hole Auger relaxation. The involvement of core-shell holes is shown to be minimal, but significant at high temperatures and low carrier concentrations. For c-BN, a maximum efficiency around 37% is estimated, exceeding all other materials, although a full MC analysis with more *ab initio* kinetics calculations are required to substantiate this. We suggest using high-temperature-resistant semiconductor (e.g., c-BN) α-voltaic to top a thermoelectric generation cycle, to increase system efficiency and mitigate the radiation damage and geometric losses. We propose a device that would meet radiation damage restrictions and temperature and heat flux requirements and predict that such a hybrid device could reach efficiencies between 28% and 22% for fuel layers between 5 and 10 μm thick.

ACKNOWLEDGMENTS

This research was in part supported by POSTECH WCU, National Research Foundation of Korea (R31-30005).

[1]G. satta, G. Cappellini, V. Olevano, and L. Reining, Phys. Rev. B. **70**, 195212 (2004).
[2]D. Jayawardane, C. Pickard, L. Brown, and M. Payne, Phys. Rev. B. **64**, 115107 (2001).
[3]S. Tanuma, C. Powell, and D. Penn, Surf. Interface Anal. **11**, 577 (1988).

[4]S. Tanuma, C. Powell, and D. Penn, Surf. Interface Anal. **17**, 911 (1991).
[5]R. R. C. D. Cress and B. J. Landi, IEEE Trans. Nucl. Sci. **55**, 1736 (2008).
[6]C. Klein, J. Appl. Phys. **39**, 2029 (1968).
[7]G. Rybicki, in *Proc. IEEE Photovoltaic Specialists Conf.* (1996), Vol. 25, p. 93.
[8]D.-Y. Qiao, X.-J. Chen, Y. Ren, and W.-Z. Yuan, J. Microelectromech. Syst. **20**, 685 (2011).
[9]L. Olsen, Energy Convers. **13**, 117 (1973).
[10]M. Chandrashekhar, C. Thomas, H. Li, G. Spencer, and A. Lal, Appl. Phys. Lett. **88**, 033506 (2006).
[11]B. Ziaja, R. London, and J. Hajdu, J. Appl. Phys. **97**, 064905 (2005).
[12]B. Ziaja, D. van der Spoel, A. Szöke, and J. Hajdu, Phys. Rev. B **64**, 214104 (2001).
[13]B. Ziaja, A. Szöke, D. van der Spoel, and J. Hajdu, Phys. Rev. B **66**, 024116 (2002).
[14]W. Brandt and G. Lapicki, Phys. Rev. A **23**, 1717 (1981).
[15]E. Fermi, Z. Phys. **29**, 315 (1924).
[16]D. Pines and D. Bohm, Phys. Rev. **85**, 338 (1952).
[17]J. Lindhard and K. Dan, Vidensk. Selsk. Mat. Fys. Medd. **28**, 1 (1954).
[18]I. Abril, R. Garcia-Molina, C. D. Denton, F. J. Pérez-Pérez, and N. R. Arista, Phys. Rev. A **58**, 357 (1998).
[19]P. Nozières and D. Pines, Nuovo Cimento **9**, 470 (1958).
[20]M. Rudd, Y.-K. Kim, D. Madison, and J. Gallagher, Rev. Mod. Phys. **57**, 965 (1985).
[21]G. Kresse and J. Hafner, Phys. Rev. B **47**, 558 (1993).
[22]G. Kresse and J. Hafner, Phys. Rev. B **49**, 14251 (1994).
[23]G. Kresse and J. Furthmller, Comput. Mater. Sci. **6**, 15 (1996).
[24]G. Kresse and J. Furthmller, Phys. Rev. B **54**, 11169 (1996).
[25]P. E. Blchl, Phys. Rev. B **50**, 17953 (1994).
[26]G. Kresse and D. Joubert, Phys. Rev. B **59**, 1758 (1999).
[27]J. P. Perdew, K. Burke, and M. Ernzerhof, Phys. Rev. Lett. **77**, 3865 (1996).
[28]J. P. Perdew, K. Burke, and M. Ernzerhof, Phys. Rev. Lett. **78**, 1396 (1997).
[29]See supplementary material at http://dx.doi.org/10.1063/1.4790506 for calculation details.
[30]S. Cipolla, Nucl. Instrum. Method B **261**, 142 (2007).
[31]S. Cipolla, Comput. Phys. Commun. **176**, 157 (2007).
[32]G. Lapicki, J. Phys. B **41**, 115201 (2008).
[33]Z. Liu and S. Cipolla, Comput. Phys. Commun. **97**, 315 (1996).
[34]W. Lochmann, Phys. Status Solidi (a) **40**, 285 (1977).
[35]J. Singh, *Physics of Semiconductors and Their Heterostructures* (McGraw-Hill, New York, 1993), p. 823.
[36]H. Bethe, Ann. Phys. (Leipzig) **5**, 325 (1930).
[37]F. Bloch, Ann. Phys. (Leipzig) **16**, 285 (1933).
[38]F. Bloch, Z. Phys. **81**, 363 (1933).
[39]P. Sigmund and A. Schinner, Nucl. Instrum. Methods Phys. Res. B **174**, 535 (2001).
[40]J. Ziegler, J. Biersack, and U. Littmark, *The Stopping and Range of Ions in Matter* (Pergamon, 1985).
[41]J. Ziegler, J. Biersack, and M. Ziegler, *SRIM—The Stopping and Range of Ions in Matter* (Ion Implantation Press, 2008).